This is an open access article published under a Creative Commons Non-Commercial No Derivative Works (CC-BY-NC-ND) Attribution License, which permits copying and redistribution of the article, and creation of adaptations, all for non-commercial purposes.

ACS APPLIED MATERIALS & INTERFACES

Research Article

Cite This: ACS Appl. Mater. Interfaces 2019, 11, 46350−46360

www.acsami.org

Air Plasma-Enhanced Covalent Functionalization of Poly(methyl methacrylate): High-Throughput Protein Immobilization for Miniaturized Bioassays

Shivani Sathish,[†] Noriko Ishizu,[‡] and Amy Q. Shen*[,†]

[†]Micro/Bio/Nanofluidics Unit, Okinawa Institute of Science and Technology Graduate University, 1919-1 Tancha, Onna-son, Kunigami-gun, Okinawa 904-0495, Japan

[‡]Mechanical Engineering and Microfabrication Support Section, Okinawa Institute of Science and Technology Graduate University, 1919-1 Tancha, Onna-son, Kunigami-gun, Okinawa 904-0495, Japan

Supporting Information

ABSTRACT: Miniaturized systems, such as integrated microarray and microfluidic devices, are constantly being developed to satisfy the growing demand for sensitive and high-throughput biochemical screening platforms. Owing to its recyclability, and robust mechanical and optical properties, poly(methyl methacrylate) (PMMA) has become the most sought after material for the large-scale fabrication of these platforms. However, the chemical inertness of PMMA entails the use of complex chemical surface treatments for covalent immobilization of proteins. In addition to being hazardous and incompatible for large-scale operations, conventional biofunctionalization strategies pose high risks of compromising the biomolecular conformations, as well as the stability of PMMA. By exploiting radio frequency (RF) air plasma and standard 1-ethyl-3-(3-(dimethylamino)propyl) carbodiimide (EDC) and *N*-hydroxysuccinimide (NHS) chemistry in tandem, we demonstrate a simple yet scalable PMMA functionalization strategy for covalent immobilization (chemisorption) of proteins, such as green fluorescent protein (GFP), while preserving the structural integrities of the proteins and PMMA. The surface density of chemisorbed GFP is shown to be highly dependent on the air plasma energy, initial GFP concentration, and buffer pH, where a maximum GFP surface density of 4×10^{-7} mol/m^2 is obtained, when chemisorbed on EDC−NHS-activated PMMA exposed to 27 kJ of air plasma, at pH 7.4. Furthermore, antibody-binding studies validate the preserved biofunctionality of the chemisorbed GFP molecules. Finally, the coupled air plasma and EDC−NHS PMMA biofunctionalization strategy is used to fabricate microfluidic antibody assay devices to detect clinically significant concentrations of *Chlamydia trachomatis* specific antibodies. By coupling our scalable and tailored air plasma-enhanced PMMA biofunctionalization strategy with microfluidics, we elucidate the potential of fabricating sensitive, reproducible, and sustainable high-throughput protein screening systems, without the need for harsh chemicals and complex instrumentation.

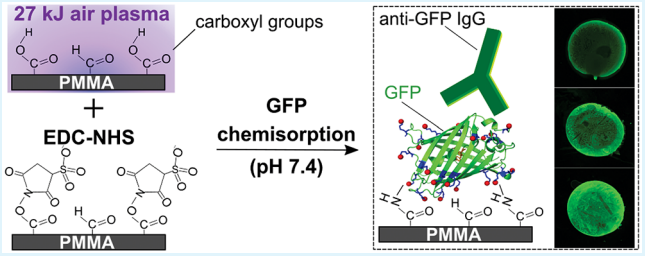

KEYWORDS: *PMMA, covalent biofunctionalization, air plasma, EDC−NHS, microfluidics, bioassay*

1. INTRODUCTION

The advent of microarray[1] and microfluidic systems[2,3] has accelerated the development of automated high-throughput screening (HTS) platforms, that allow parallel multivariate analysis of chemical[4] and biochemical[5] compounds. Owing to their high optical transparency and amenability to thermo- and vacuum-forming, thermoplastics have been used for large-scale fabrication of these systems.[6] In addition to its robust mechanical and chemical properties, the thermal decomposition of poly(methyl methacrylate) (PMMA) to its monomeric constituent (MMA) enables the fabrication of durable yet recyclable microchips at a low-cost.[7] However, the low surface energy and chemical inertness of PMMA decreases its compatibility with biomolecules, such as DNA and proteins. The hydrophobicity of the PMMA surfaces triggers biomolecule physisroption via hydrophobic interactions that not only increases non-specific adsorption but also enhances biomolecule denaturation.[8] Several efforts are being made to reduce biomolecule physisorption by chemically treating PMMA surfaces so as to generate functional groups that enable covalent coupling of biomolecules, with the main aim of preserving biomolecular conformations and biofunctional activities.

The most commonly used chemical treatments rely on aminolysis[9,10] or hydrolysis[11,12] to generate amine- or carboxyl-terminated PMMA surfaces, respectively. These methods require stringent and time-consuming acid or base treatments which not only change the topography and transparency of the

Received: August 23, 2019
Accepted: November 13, 2019
Published: November 13, 2019

See https://pubs.acs.org/sharingguidelines for options on how to legitimately share published articles.

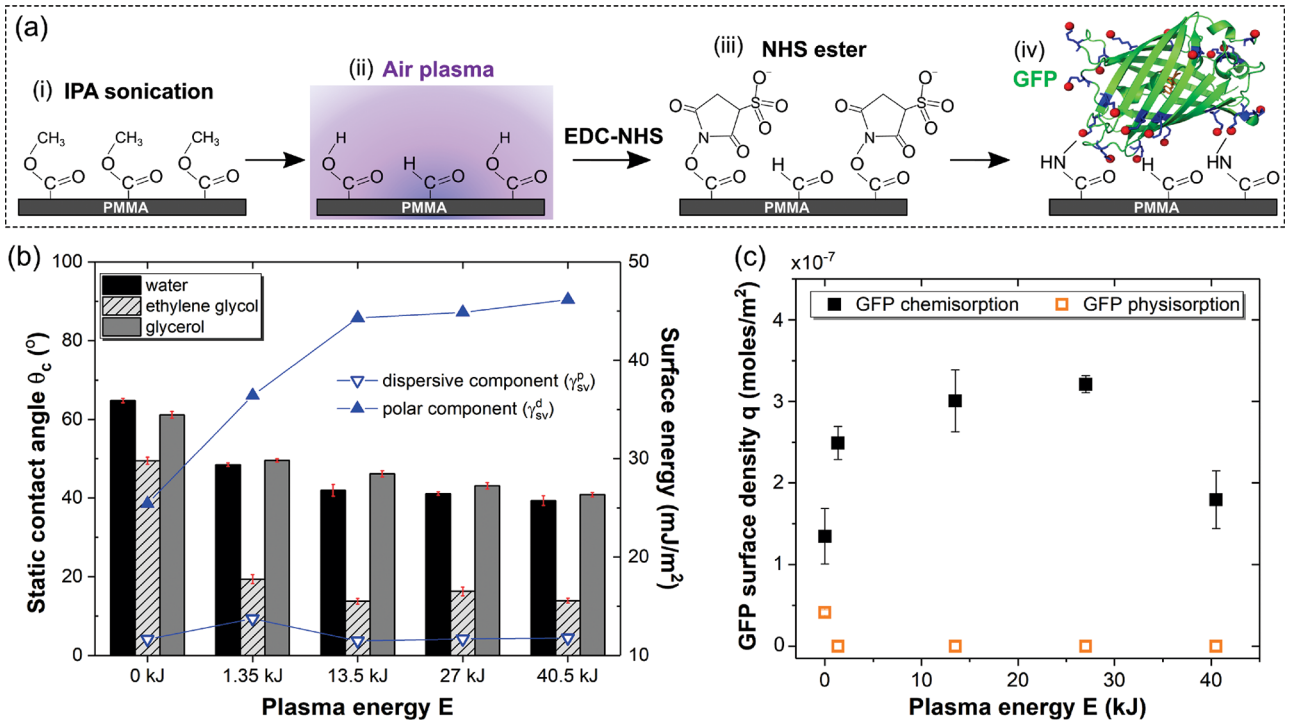

Figure 1. (a) Schematic illustrating the covalent immobilization of GFP on air plasma-activated PMMA. The GFP structure in (iv) was obtained from the Protein Databank (PDB 1GFL) and modified using PyMOL open-source visualization software. The blue rods and red spheres in the GFP structure indicate the lysine residues and primary amine groups, respectively. (b) Evolution of static contact angles and polar and dispersive solid−vapor interfacial energies of plasma activated PMMA surfaces as a function of air plasma energy. (c) GFP surface density plotted as a function of air plasma energy. GFP surface density was calculated from the standard curve in Figure S1. Standard deviations have been calculated for three independent experiments (n = 3) and within the symbols for the orange data points.

PMMA substrates but also pose significant safety issues during large-scale treatments. Alternatively, Ortiz et al. recently demonstrated a less harsh method that relies on deposition of silica nanoparticles on PMMA microchips for subsequent functionalization with conventional silane chemistry.[13] Although the microchips were shown to be biocompatible with unaltered optical properties, the described method is not practical for mass production.

In contrast, highly reactive ionized gas plasmas such as ammonia, argon, oxygen, and so on, have been exploited to generate active functional groups on PMMA surfaces, thereby increasing the surface energy and hydrophilicity of the surfaces, without the use of toxic chemicals.[14] Carbondioxide plasma has been proven to efficiently add active carboxyls on surfaces of silicon based substrates like glass for subsequent biofunctionalization of proteins.[15] Conversely, due to the presence of innate carbon atoms on the surfaces of PMMA, ozone coronas coupled with UV (ultraviolet) irradiation have been used to generate a mixture of polar groups (carboxyls, ketones, hydroxyls) to covalently couple DNA fragments to PMMA surfaces.[16] However, UV−ozone oxidation was shown to confer a blue tint to the PMMA substrate which altered its intrinsic fluorescence properties. Alternatively, the reaction of radiofrequency discharge (RF) oxygen[17] and water vapor plasma[18] with PMMA surfaces was shown to generate a high density of polar groups, without altering the bulk properties. These surfaces were subsequently coated with either thin films of acrylic acid[19] or organosilanes[18] for further covalent coupling with DNA and proteins. While the high susceptibility to hydrolysis in ambient conditions renders silanated surfaces unstable during long-term use, a thin-film approach is not scalable. Recently, owing to their simplicity, air plasmas created by dielectric barrier discharge (DBD)[20−22] and atmospheric-pressure plasma jets (AAPJ)[14] have been exploited to modify surfaces of thermoplastics such as polytetrafluoroethylene (PTFE) for chemical and biomolecule coatings. Although these air plasma jets generate polar functional groups with similar efficiencies as oxygen plasma, their effects are localized, creating nonuniform distributions of functional groups. In lieu to atmospheric pressure discharges, low-pressure radiofrequency (RF) air plasma has become increasingly popular for surface hydrophilization of polymers, including PMMA, to increase surface wettability for various applications.[16,23] However, the efficacy of RF air plasmas to generate sufficient functional groups on PMMA for biomolecule immobilization is unclear.

To address the various challenges of achieving reproducible PMMA biofunctionalization, we took advantage of the ability of RF air plasmas to generate a mixture of polar functional groups such as carboxyls, hydroxyls, and carbonates on PMMA surfaces and selectively exploited the carboxyls for covalent coupling of proteins via simple 1-ethyl-3-(3-(dimethylamino)-propyl) carbodiimide (EDC) and *N*-hydroxysuccinimide (NHS) chemistry. Owing to its intrinsic ability to exhibit changes in fluorescence emission when exposed to protein-denaturating conditions, we used green fluorescence protein (GFP) as a model protein system to quantify the preservation of biomolecular structure and biofunctionality following immobilization. Here, we demonstrated that the functional groups generated on PMMA surfaces when exposed to air plasma can be subsequently exploited to decrease non-specific hydrophobic adsorption while increasing selective chemisorp-

DOI: 10.1021/acsami.9b14631
ACS Appl. Mater. Interfaces 2019, 11, 46350−46360

tion of GFP. Additionally, we found that the GFP surface density can be tuned as a function of air plasma energy, where we obtained a maximum surface density of 4×10^{-7} mol/m^2, which is within the desirable protein surface density range (10^{-9} to 10^{-7} mol/m^2), to mimic surfaces of cells.[24] Binding studies were performed with GFP specific antibodies, where we observed that the chemisorption and biofunctionality of the chemisorbed GFP is highly sensitive to buffer pH. Finally, we biofunctionalized PMMA microfluidic antibody assay devices using the described strategy and successfully detected clinically significant concentrations of *Chlamydia trachomatis* specific antibodies. By integrating the described air plasma-enhanced PMMA protein-functionalization method with microfluidics, we demonstrated the potential of creating reproducible and recyclable PMMA microchips for applications in biochemical screening, on a large scale.

2. EXPERIMENTAL SECTION

2.1. Materials. PMMA sheets (Shinkolite acrylic sheet) was purchased from Mitsubishi Chemical Corporation, Japan. EDC, NHS, isopropyl alcohol (IPA), ethylene glycol, glycerol, phosphate-buffered saline (PBS), 2-(*N*-morpholino)ethanesulfonic acid (MES), bovine serum albumin (BSA), and Tween 20 were purchased from Nacalai Tesque, Inc., Japan. Recombinant green fluorescent protein (rGFP, 632373) was purchased from Takara Bio, Japan. Alexa Fluor 488 conjugated GFP rabbit polyclonal antibody (A-21311), Alexa Fluor 555 rabbit anti-goat secondary antibody (A-21431), Alexa Fluor 488 chicken anti-goat secondary antibody, and DyLight 550 conjugated streptavidin, were purchased from Thermo Fischer Scientific, Japan. Recombinant *Chlamydia trachomatis* major outer membrane protein (MOMP) (ab226442) and FITC-labeled anti-MOMP polyclonal antibody (ab30951) were purchased from Abcam, Japan. Human plasma was provided by Sysmex Corporation, Japan.

2.2. PMMA Surface Treatment, GFP Immobilization, and Bioassay. *2.2.1. Air Plasma Treatment.* PMMA sheets (2 mm thickness) were cut into strips (37.5 mm × 25 mm) using a carbon dioxide (CO_2) laser scriber (VLS 3.60, Universal Laser Systems, USA) and briefly rinsed with 98% IPA and milli-Q water. The PMMA strips were then sonicated in 50% aqueous IPA at 43 kHz, 25 °C for 10 min, rinsed with 98% IPA followed by milli-Q water, and dried well under a constant stream of nitrogen (N_2) gas. The size of the PMMA strips were kept constant for all surface treatment and characterization experiments elaborated in this article. The surfaces of IPA-cleaned PMMA strips were treated with air plasma for varying time intervals (30 s, 5, 10, and 15 min) at a fixed RF power of 45 W and 60 L/min flow rate, at 0.25 Torr base pressure, using a high RF power expanded Plasma Cleaner (PDC-001-HP (115 V), Harrick Plasma, USA) and a dry scroll vacuum pump (IDP-3, 60 kHz model, Agilent Technologies, USA) for flow rate control. The plasma-treated PMMA surfaces were immediately incubated in a 50 mM solution of EDC−NHS (1:1) in 100 mM MES buffer (pH 5), for 20 min for surface activation (Figure 1a(i)−(iii)). The activated PMMA strips were rinsed with milli-Q water and dried with a puff of N_2.

2.2.2. GFP Chemisorption Studies. For the GFP immobilization studies, 0.6 μL droplets of GFP with varying concentrations (1−50 μg/mL), either in 0.01 M PBS buffer (pH 7.4) or 0.01 M MES buffer (pH 6), were incubated on the activated PMMA surfaces for 15 min (Figures 1a(iv) and 2). The unbound GFP molecules were removed by rinsing the biofunctionalized PMMA with a wash buffer consisting of 0.01 M PBS and 0.05% Tween 20.

2.2.3. GFP-Antibody Binding Studies. Binding studies between the immobilized GFP and anti-GFP antibodies were carried out to semi-quantitatively analyze the biofunctionality of the immobilized GFP. First, the GFP-functionalized PMMA surfaces were blocked with 1% weight/volume of BSA in 0.01 M PBS buffer for 30 min at room temperature. The blocked PMMA surfaces were incubated with a 3 μg/mL solution of anti-GFP antibodies in 0.01 M PBS for 1 h at room

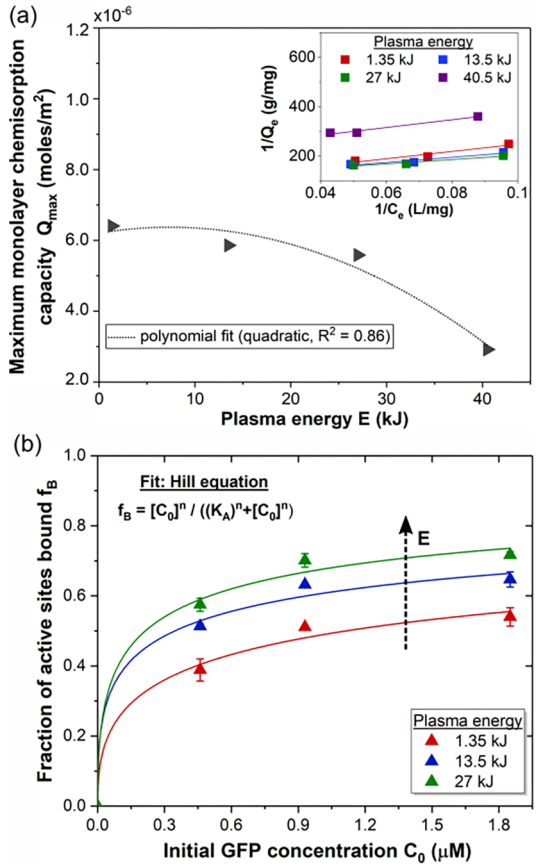

Figure 2. (a) Maximum monolayer adsorption capacity of PMMA (Q_{max}) plotted as a function of plasma energy (E). The dotted lines depict the poynomial (quadratic) fit for the data points. Inset: Linearized Langmuir isotherm analyses of GFP chemisorbed on PMMA treated with EDC−NHS and different plasma energies. Solid lines depict the linear fits of the data points. Error bars are within the symbols (n = 3). (b) Fraction of active sites bound (f_B) with GFP plotted as a function of initial GFP concentration (C_0) on EDC−NHS-treated PMMA substrates exposed to 1.35, 13.5, and 27 kJ RF air plasma, respectively. Solid lines depict data fitting with the Hill equation (n = 3, R^2 = 0.99).

temperature (Figure 3). The PMMA surfaces were rinsed well with wash buffer to remove any non-specifically bound antibodies.

2.2.4. Microfluidic Chlamydia-Specific IgG Assay. PMMA strips were exposed to 27 kJ of air plasma and activated with EDC−NHS as described in section 2.2.1. 0.6 μL droplets of 1.25 μM MOMP in PBS buffer (pH 7.4) were incubated on the activated surfaces for 15 min. The unbound MOMP fragments were washed with wash buffer (0.01 M PBS and 0.05% Tween 20). The MOMP-functionalized PMMA strips served as the base of the microfluidic channel. 2D microchannel layouts (1 cm length × 1.5 mm width) were etched through 53 μm thick layers of double-sided (ds) adhesive tapes with a CO_2 laser scriber, using a previously described method.[25] These etched ds-tapes were bonded to the MOMP-functionalized PMMA strips on one side and IPA-cleaned PMMA strips on the other side to complete the microfluidic device (Figure 4a). The bare surfaces of the PMMA microchannels were blocked with 1% weight/volume of BSA to prevent non-specific adsorption. Either human plasma diluted with PBS buffer (1:2) or PBS buffer samples (100 μL) were doped with varying concentrations of anti-MOMP IgGs (0.83−13.3 nM) and pipetted into the inlet of the microchannels. The devices were incubated for 1 h for the human plasma samples and 15 min for PBS samples and washed to remove unbound IgGs. Blank reactions were carried out by flowing IgG-doped samples through BSA-blocked microchannels without MOMP, and incubated for the same amount

DOI: 10.1021/acsami.9b14631
ACS Appl. Mater. Interfaces 2019, 11, 46350−46360

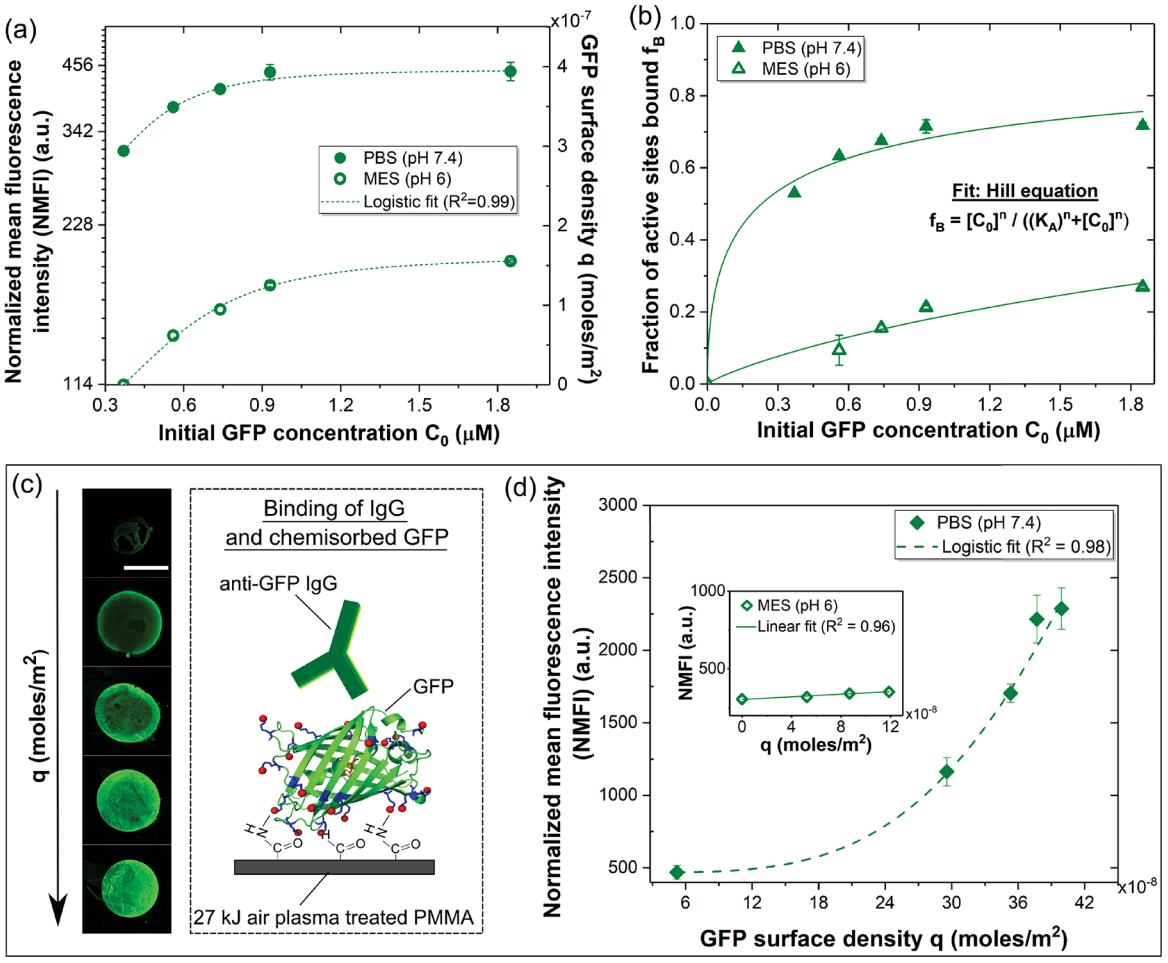

Figure 3. (a) Fluorescence intensity of GFP chemisorbed on EDC−NHS-treated PMMA exposed to 27 kJ air plasma, plotted against initial GFP concentration (C_0), immobilized at pH 7.4 and pH 6 (n = 3). (b) Fraction of active sites bound plotted against C_0, for GFP chemisorbed at pH 7.4 and 6. Solid lines depict data fitting with the Hill equation (R^2 = 0.98 (pH 7.4); 0.93 (pH 6); n = 3). (c) Fluorescence images and schematic of IgG bound to increasing surface density of chemisorbed GFP. Scale bar is 500 μm. (d) Binding of IgG to chemisorbed GFP as a function of GFP surface density q at pH 7.4 and (inset) pH 6 (n = 3).

of times. Finally, fluorescently labeled secondary IgGs (33 nM) specific to the anti-MOMP IgGs were pipetted into the channels and incubated for 15 min. Following washing, the microfluidic devices were imaged via fluorescence microscopy.

2.3. Surface Characterization. *2.3.1. Contact Angle Measurements.* Static contact angles of 3 μL droplets of milli-Q water, ethylene glycol, and glycerol, dispensed at a drop rate of 3 μL/s at 3 different positions on each plasma-treated PMMA surface, were cumulatively measured by the static sessile drop method (Attension Theta tensiometer, Biolin Scientific, U.S.A.) to determine the surface wettability of the PMMA surfaces treated with different plasma energies.

2.3.2. X-ray Photoelectron Spectroscopy. X-ray photoelectron spectroscopy (XPS) analyses were performed using AXIS-ULTRA DLD (Kratos Analytical Inc., Manchester UK) with a monochromated Al Kα X-ray source with a power of 150 W (15 kV, 10 mA) to acquire surface atomic concentrations of carbon (C), oxygen (O), nitrogen (N), and silicon (Si) on the plasma-treated PMMA strips. PMMA sheets were cut into 1 cm × 1 cm squares for the measurements. Survey spectra were measured at pass energy of 160 eV, and high-resolution spectra were measured at 20 eV in an analysis area of approximately 300 μm × 700 μm with the hybrid lens and slot modes, with a takeoff angle of 0° to the surface normal. The charge neutralizer with low-energy electrons was used to compensate the surface charging. The XPS data were acquired from 2 independent sets of samples with 5 sweeps in each sample. Data processing was performed using CasaXPS processing software. The atomic concentrations were calculated using the sensitivity factors supplied by the manufacturer. Binding energies were calibrated using hydrocarbon C 1s at 284.6 eV.

2.4. Data Analysis. The PMMA strips biofunctionalized with GFP and/or the anti-GFP antibodies were imaged under a FITC filter using a Nikon Ti-E epifluorescence microscope equipped with a CCD camera (Orca Frash v4.0, Hamamatsu photonics). All samples were imaged at a fixed exposure time of 10 s. The raw images captured for each condition were analyzed and processed using ImageJ (NIH, USA). First, the large spacial variations of the background pixel intensities were subtracted from all the raw fluorescence images using the built-in rolling-ball background subtraction algorithm in ImageJ. A pixel radius of 300 pixels, greater than the largest signal that was not part of the background, was used for all images for the background subtraction. Following background subtraction, the mean pixel intensity per 1 μm^2 area for the selected region of interest (ROI) that encapsulated the entire droplet, was extracted for each image. Next, a standard curve relating the normalized mean pixel intensities and the surface density of immobilized GFP molecules normalized to the total droplet area (mol/m^2) was generated. Finally, the surface density of immobilized GFP on the different surface treated PMMA strips was estimated by comparing the extracted normalized mean pixel intensities of the respective images, with the GFP surface density standard curve (Figure S1). The microfluidic anti-MOMP IgG assay devices were imaged and analyzed in a similar fashion as explained above. After background subtraction, the mean fluorescence intensity ratios, i.e., the ratio of mean pixel intensity per 1 μm^2 area for the

DOI: 10.1021/acsami.9b14631
ACS Appl. Mater. Interfaces 2019, 11, 46350−46360

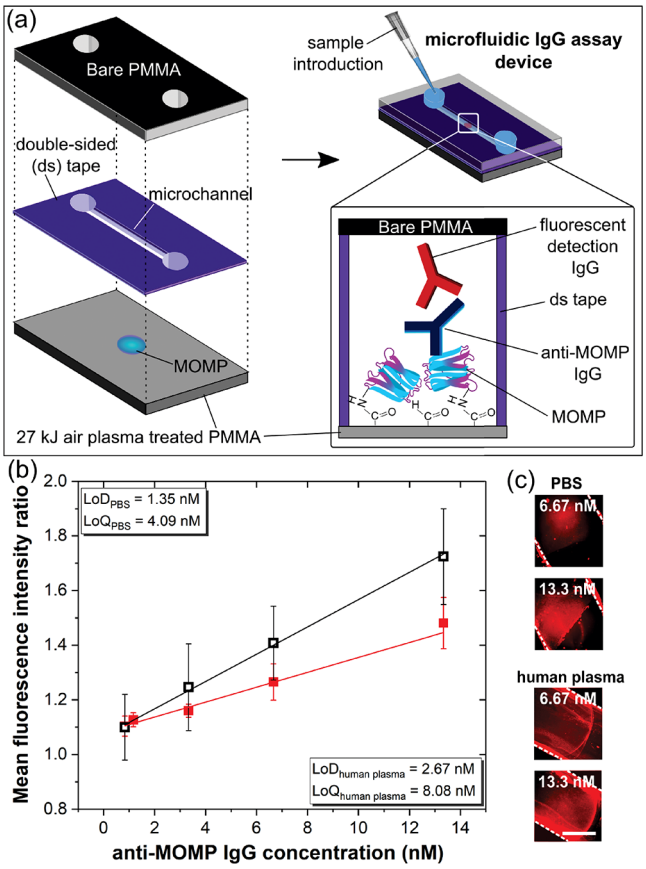

Figure 4. (a) Schematic illustrating the fabrication of the microfluidic anti-MOMP IgG assay device patterned with major outer membrane protein (MOMP) of *Chlamydia trachomatis*. Inset describes the binding architecture of biomolecules in the fluorescent-based IgG assay, in the microchannel. (b) Biding curve depicting the linear range of anti-MOMP IgG concentrations detected in the microfluidic devices (R^2 = 0.96 (red) and 0.99 (black), n = 3). (c) Images of the fluorescence-based anti-MOMP IgG assay. Dotted lines delineate the microchannel walls. Scale bar is 750 μm.

assay to that of the blank reactions, were calculated and used for quantifying the assay. All data have been graphically depicted using OriginPro2017 (OriginLab, USA). Additionally, the images were processed post quantification to increase the contrast through linear modifications in ImageJ for visual depiction.

3. RESULTS AND DISCUSSION

3.1. Air Plasma-Enhanced Covalent Chemisorption of GFP on PMMA. The immobilization of proteins on the surfaces of chemically inert plastics such as poly(methyl methacrylalte) (PMMA) is driven primarily by hydrophobic attraction. The immobilization of proteins via hydrophobic interactions increases the probability of protein unfolding and denaturation.[8] Additionally, as these interactions are non-covalent, they are affected by various environmental conditions such as water content, ionic strength of the buffer, and so on. Hence, the proteins can be easily dissociated from the plastic surfaces when exposed to different buffers and fluid samples. Furthermore, the hydrophobic adsorption of proteins on the plastic surfaces, triggers protein unfolding and denaturation.[8] To achieve immobilization of proteins with preserved structural integrity, we demonstrated the potential of utilizing radio frequency (RF) air plasma to enable covalent immobilization (chemisorption) of proteins on PMMA, achieved by linking surfaces of proteins to PMMA without altering bulk protein conformations.

Here, we exposed the surfaces of IPA-cleaned PMMA to different energies of RF air plasma by changing plasma exposure times (30 s−15 min), with a fixed RF power of 45 W, to generate a mixture of polar functional groups such as carboxylic acids (RCO_2H) and hydroxyl ions (OH^-) (schematic in Figure 1a(i),(ii)). The generated carboxyl groups were selectively exploited to covalently link with the primary amines (NH_2) of lysine residues on the surfaces of GFP via EDC−NHS chemistry (Figure 1a(iii),(iv)). GFP[26,27] was used as the model protein to (i) investigate the specificity of covalent immobilization, since the surface of GFP has a large number of hydrophobic sites and interactions with PMMA are predominantly hydrophobic, and (ii) monitor the changes in conformation of GFP following immobilization, by tracking the change in its intrinsic fluorescence emission.

First, the change in the hydrophobic nature of PMMA surfaces was investigated by monitoring the surface wettability of PMMA when exposed to different plasma energies, by measuring the respective static contact angles (θ_c) of water, ethylene glycol, and glycerol for each treated PMMA substrate (bars in Figure 1b). The surfaces of PMMA sonicated in IPA are relatively hydrophobic with θ_c = 65° and became increasingly hydrophilic with increasing plasma energy (1.35 kJ < E < 27 kJ). The contact angles remained relatively constant after E > 13.5 kJ. This effect of apparent saturation of contact angles is consistent with previous literature that indicate the saturation of functional groups on PMMA surfaces at specific plasma energies. With further increase in plasma energy, the ions penetrate into the bulk of the PMMA, thereby modifying bulk properties.[14,28] As contact angle measurements are indicative of intrinsic effects on the surfaces of materials, the saturation of functional groups on PMMA surfaces when exposed to air plasma, is depicted by the saturation of contact angles at E = 13.5 kJ. However, the surface roughness of PMMA was observed to be unchanged when exposed to such low energies of air plasma (Figure S2). To estimate the free energy of the PMMA surfaces, the contact angles (θ_c) for each test liquid was interrelated with the solid−liquid (γ_{sl}), solid−vapor (γ_{sv}), and liquid−vapor (γ_{lv}) interfacial energies using the Young's equation (eq 1) and the combining rule proposed by the Owens, Wendt, Rabel, and Kaelble (OWRK) model (eq 2):[29,30]

$$\gamma_{lv} \cos\theta_c = \gamma_{sv} - \gamma_{sl} \quad (1)$$

$$\gamma_{sl} = \gamma_{sv} + \gamma_{lv} - 2\left(\sqrt{\gamma_{sv}^{d}\gamma_{lv}^{d}} + \sqrt{\gamma_{sv}^{p}\gamma_{lv}^{p}}\right) \quad (2)$$

where, γ_{sv}^{d}, γ_{sv}^{p} and γ_{lv}^{d}, γ_{lv}^{p} (mJ/m^2) are the dispersive and polar components of the solid−vapor, and liquid−vapor interfacial energies, respectively. The values of γ_{lv}^{d} and γ_{lv}^{p} for the three test liquids are displayed in Table 1. Equations 1 and 2 were first combined to form eq 3, and then rearranged to be represented

Table 1. Polar and Dispersive Components of the Liquid−Vapor Interfacial Energies of the Three Test Liquids Employed in the OWRK Model[31]

liquids	γ_{lv} (mJ/m^2)	γ_{lv}^{p} (mJ/m^2)	γ_{lv}^{d} (mJ/m^2)
water	72.8	51.0	21.8
ethylene glycol	47.7	16.8	30.9
glycerol	63.4	26.4	37.0

DOI: 10.1021/acsami.9b14631
ACS Appl. Mater. Interfaces 2019, 11, 46350−46360

Table 2. X-ray Photoelectron Spectroscopic (XPS) Analysis of Surface Functional Groups Generated on PMMA as a Function of Air Plasma Energy (E)

		peak composition of the C 1s spectra			
plasma energy E (kJ)	O/C ratio	C 1s-1 %[a]	C 1s-1 %[b]	C 1s-1 %[c]	C 1s-1 %[d]
binding energy (eV)		284.6	286.3	288.6	287.2
0	0.33333	48	20 ± 4	14.5 ± 1.5	1.5 ± 1.5
1.35	0.40845	40.5 ± 1.5	20 ± 1	18.5 ± 1.5	3.5 ± 0.5
13.5	0.44928	41 ± 1	21.5 ± 1.5	20.5 ± 2.5	2 ± 1
27	0.42857	40.5 ± 2.5	21.5 ± 0.5	20 ± 3	3 ± 1
40.5	0.42857	39.5 ± 1.5	22 ± 1	19 ± 2	2.5 ± 0.5

[a]C 1s-(1−6) correspond to carbon (C)-atoms involved in the bonds of hydrocarbon (C−C/C−H). [b]C 1s-(1−6) correspond to carbon (C)-atoms involved in the bonds of methoxy (O−CH_3). [c]C 1s-(1−6) correspond to carbon (C)-atoms involved in the bonds of carboxyl (O−(C═O)). [d]C 1s-(1−6) correspond to carbon (C)-atoms involved in the bonds of free carbonyl (C═O^-) groups. Peak composition values have been averaged for five sweeps for each tested condition, over two sets of independent experiments.

in the linear form (eq 4), where the plot of $0.5\gamma_{lv}(1 + \cos\theta_c)/\sqrt{\gamma_{lv}^d}$ versus $\sqrt{\gamma_{lv}^p/\gamma_{lv}^d}$ yields a slope of $\sqrt{\gamma_{sv}^p}$ and an intercept of $\sqrt{\gamma_{sv}^d}$.

$$\sqrt{\gamma_{sv}^d\gamma_{lv}^d} + \sqrt{\gamma_{sv}^p\gamma_{lv}^p} = 0.5\gamma_{lv}(1 + \cos\theta_c) \quad (3)$$

$$\sqrt{\gamma_{sv}^d} + \sqrt{\gamma_{sv}^p}\sqrt{\frac{\gamma_{lv}^p}{\gamma_{lv}^d}} = \frac{0.5\gamma_{lv}(1 + \cos\theta_c)}{\sqrt{\gamma_{lv}^d}} \quad (4)$$

The individual dispersive and polar components of the solid−vapor surface energies of PMMA substrates when exposed to different plasma energies were extracted from the linear graph, as shown in Figure S3. As seen from the closed blue triangles in Figure 1b, the gradual increase and apparent saturation of γ_{sv}^p indicated that air plasma exposure increased the polarity of PMMA when exposed to plasma energy E < 27 kJ. This depicts that the surfaces of PMMA become increasingly hydrophilic with increasing plasma energy, owing to the increase in oxygen incorporation on the PMMA surfaces as a consequence of air plasma activation, validated by the changes in oxygen to carbon ratio (O/C) obtained by XPS analysis (Table 2). Although the O/C ratio was seen to reach saturation when E > 27 kJ, the distribution of polar functional groups, obtained from the deconvulated C 1s XPS spectra,[28] was seen to vary with respect to the different plasma energies. In particular, the proportion of carboxyl groups and free carbonyl groups were highest on the 13.5−27 kJ plasma-activated PMMA and seen to decrease with further increase in plasma energy. These results are consistent with previously described research[19,23] where a steady decline of carboxyl groups was observed after a critical plasma energy, due to plasma-induced oxidation of PMMA surfaces by free oxygen radicals.

To verify the carboxyl generation with exposure to air plasma, the plasma-treated PMMA surfaces were activated by EDC−NHS and coupled with a fixed concentration (12.5 μg/mL) of GFP (i.e., chemisorption). In parallel, the same concentration of GFP was added to plasma-treated PMMA surfaces without EDC−NHS activation (i.e., physisorption). The surfaces were washed to remove unbound GFP and imaged to quantify the surface density of immobilized GFP, by comparing the fluorescence intensities with a standard curve (Figure S1). As depicted by the orange squares in Figure 1c, ≈4.5×10^{-7} mol/m^2 of GFP was observed to physisorb on IPA-cleaned PMMA, owing to the hydrophobicity of the surface (θ_c = 65°) that triggered hydrophobic physisorption on GFP. On the contrary, as predicted by the high γ_{sv} (blue triangles in Figure 1b), the high surface energy of the PMMA surfaces obtained by air plasma treatment reduced non-specific physisorption of GFP, where the GFP surface density was lower than the detectable limit of the microscope (Figure S1) for all plasma energies. However, the surface density of chemisorbed (covalently coupled) GFP on EDC−NHS-treated surfaces was observed to be 2- to 3-fold higher for EDC−NHS-treated plasma-activated PMMA (black squares in Figure 1c). As EDC−NHS reaction is specific to carboxyl groups, the ability of EDC−NHS-activated, plasma-treated PMMA surfaces to chemisorb GFP proves the presence of carboxyl groups on the PMMA surfaces, in response to air plasma exposure.

On further examination of the solid squares in Figure 1c, the GFP surface density was significantly higher when chemisorbed (with EDC−NHS) on IPA-cleaned surfaces when compared to physisorption (no EDC−NHS). This apparent difference is a result of the high proportion of carboxyl groups (16%) generated on PMMA surfaces during IPA sonication when compared to pristine PMMA (7%, Figure S4), as predicted by previous studies.[32,33] As the penetration depth of X-rays used in XPS is usually between 10−100 nm,[34] the relative percentages of the functional groups do not provide an absolute estimate of the functional groups present on the outermost surface of PMMA, that is accessible to the biomolecules. Hence, the reduction of carboxyl groups cannot be significantly proven by XPS data alone. However, the immobilization efficiency of the biomolecules is a direct measure of functional groups on the surface of PMMA. Therefore, we quantified the GFP surface density as a method to characterize the proportion of carboxyl groups on air-plasma-activated PMMA, treated with EDC−NHS. As seen in Figure 1c, the surface density of chemisorbed GFP (with EDC−NHS) was observed to increase with increasing plasma energy up to 27 kJ, after which the surface density was seen to decrease. As initially, depicted in Table 2, PMMA surfaces treated with E > 27 kJ air plasma showed a decrease in proportion of carboxyl and carbonyl groups. Correspondingly, the surface density of chemisorbed GFP decreased when exposed to plasma energies of E > 27 kJ, verifying that the GFP chemisorption was indeed driven by EDC−NHS-mediated carboxyl−amine coupling. Additionally, as the XPS measurements are carried out over a period of a few hours, the proportion of functional groups observed are a measure of the functionality of PMMA in its relaxed state. The presence of a

DOI: 10.1021/acsami.9b14631
ACS Appl. Mater. Interfaces 2019, 11, 46350−46360

Table 3. Langmuir Adsorption Isotherm Parameters for GFP Chemisorption on EDC−NHS-Treated Plasma-Activated PMMA as a Function of Air Plasma Energy

				q ($\times 10^{-7}$ mol/m^2)		
E (kJ)	b (L/mg)	Q_{max} (mg/g)	linearity (R^2)	C_0 = 0.46 μM	C_0 = 0.93 μM	C_0 = 1.85 μM
1.35	0.06849	0.0099	0.94	2.49 ± 0.20	3.27 ± 0.02	3.46 ± 0.17
13.5	0.10416	0.00906	0.93	3.0 ± 0.04	3.7 ± 0.01	3.79 ± 0.13
27	0.1321	0.00864	0.95	3.21 ± 0.10	3.92 ± 0.11	4.0 ± 0.05
40.5	0.14119	0.00451	0.97	1.79 ± 0.04	2.19 ± 0.11	2.2 ± 0.06

considerable proportion of carboxyl groups (Table 2) demonstrate that the PMMA surfaces are relatively stable after a few hours. However, the chemisorption of GFP is the most efficient within a few minutes of plasma exposure and EDC−NHS activation.

3.2. GFP Chemisorption with Tunable Affinities on Air Plasma-Activated PMMA Treated with EDC−NHS. Efficient covalent immobilization of GFP on activated PMMA is achieved when GFP is irreversibly chemisorbed on a finite number of carboxyl sites on the PMMA surface. Assuming that GFP molecules do not aggregate, the carboxyl sites on activated PMMA surfaces would saturate at equilibrium, forming a packed monolayer of GFP. Under these conditions, the chemisorption of GFP on EDC−NHS-treated, plasma-activated PMMA surfaces, can be quantified by the Langmuir adsorption isotherm model.[35,36] Here, the behavior of the EDC−NHS-activated PMMA, treated with increasing RF plasma energies, was described using the linearized form of the Langmuir adsorption isotherm:

$$\frac{1}{Q_e} = \frac{1}{Q_{max}} + \frac{1}{bQ_{max}} \cdot \frac{1}{C_e} \tag{5}$$

where Q_{max} (mg/g) is the maximum monolayer adsorption capacity of PMMA and b (L/mg) is the Langmuir equilibrium chemisorption constant. The values of Q_{max} and b for GFP chemisorption on activated PMMA treated with different plasma energies were extracted from the slopes and intercepts of the linear plots of $1/Q_e$ versus $1/C_e$ (inset of Figure 2a) according to eq 5 and listed in Table 3. Q_e (mg/g) is the amount of GFP chemisorbed on PMMA at equilibrium and C_e (mg/L) is the GFP equilibrium concentration, estimated from eqs 6 and 7, for different initial GFP concentration, C_0 (M):

$$Q_e = \frac{qA_{drop}M_w}{V_{drop} \cdot \rho} \tag{6}$$

$$C_e = \frac{(q_0 - q)A_{drop}M_w}{V_{drop}} \tag{7}$$

where $q_0 = C_0V_{drop}/A_{drop}$ (mol/m^2) is the initial GFP surface density, and q (mol/m^2) is the GFP surface density at equilibrium, i.e., at saturation, estimated from the standard curve in Figure S1. A_{drop} (m^2) and V_{drop} (L) are the areas and volumes of the GFP droplet, M_w = 27 kDa is the molecular weight of GFP, and ρ = 1180 g/L is the density of PMMA.

As shown in Table 3, the high linearity of the Langmuir adsorption fits (linearity, R^2 = 0.93−0.97), verifies that monolayers of GFP are chemisorbed on EDC−NHS-activated PMMA when treated with RF air plasma (inset of Figure 2a). However, a decrease in the maximum monolayer adsorption capacity of the PMMA surfaces (Q_{max}, mol/m^2) as a function of plasma energy was seen (Figure 2a). This decrease in adsorption capacity correlated with the decrease of carboxyl groups seen when PMMA is exposed to E > 27 kJ of air plasma, as illustrated previously in Table 2. Owing to the large Q_{max} for 1.35 < E < 27 kJ treated PMMA surfaces, increased GFP surface density was consequently obtained, when activated with EDC−NHS (solid quares in Figure 1b). In contrast, the chemisorption of GFP on IPA-cleaned PMMA treated with EDC−NHS did not depict linearity with the Langmuir adsorption model (linearity, R^2 = 0.50, data not shown), indicating inefficient chemisorption of GFP, and larger non-specific physisorption of aggregates. Therefore, a mixture of chemisorbed monolayers and aggregates could contribute to the high GFP surface density observed in Figure 1c, for IPA-cleaned PMMA surfaces.

As the EDC−NHS-mediated coupling of proteins and carboxyl functional groups is highly time-sensitive (low stability at room temperature),[37] the differences in chemisorption efficiencies of GFP on EDC−NHS-treated, plasma-activated PMMA within a fixed reaction time of 15 min, was investigated. As initially seen in Figures 1b and 2a, 1.35−27 kJ of air plasma-enabled high GFP chemisorption when treated with EDC−NHS. Therefore, these PMMA treatment conditions were chosen to further investigate the effect of initial concentrations of GFP (C_0) on the GFP surface densities (q). The GFP surface density (q) was seen to increase with increasing C_0 for all chosen treatment conditions and appeared to reach saturation when $C_0 \geq$ 0.93 μM (Figure S5). As predicted by the high Q_{max} values (Figure 2a), q was seen to logarithmically increase with plasma energy from 1.35 to 27 kJ for all C_0. However, a difference in the rate of GFP surface saturation was observed between these surfaces. The rate of GFP chemisorption is predominantly inflenced by the affinity between the PMMA surfaces and the GFP molecules. The Hill−Langmuir equation (eq 8)[38] was used to correlate the differences in GFP saturation with the affinity of PMMA to chemisorb GFP, when exposed to plasma energies between 1.35−27 kJ treated with EDC−NHS:

$$f_B = \frac{[C_0]^n}{[C_0]^n + K_A^n} \tag{8}$$

where $f_B = q/Q_{max}$ is the fraction of active sites on PMMA (Q_{max}) bound with GFP (q). K_A is the apparent microscopic dissociation constant, and n is the Hill cooperativity coefficient. K_A is the GFP concentration required to saturate half of the available sites on PMMA and is a measure of the affinity of PMMA to GFP.

As shown in Table 4, K_A decreases with increasing plasma energy from 1.35 to 27 kJ, indicating that a low concentration of GFP (C_0 = 0.21 μM) is sufficient to saturate half of the available sites on EDC−NHS-treated PMMA surfaces exposed to 27 kJ of air plasma, when compared to lower plasma energies ($C_0 \geq$ 0.35 μM). As a consequence, the PMMA

DOI: 10.1021/acsami.9b14631
ACS Appl. Mater. Interfaces 2019, 11, 46350−46360

Table 4. Hill–Langmuir Equation Parameters for GFP Chemisorption on Activated PMMA as a Function of Air Plasma Energy

plasma energy (kJ)	K_A (μM)	n
1.35	1.11 ± 0.17	0.44 ± 0.11
13.5	0.35 ± 0.11	0.41 ± 0.12
27	0.21 ± 0.09	0.48 ± 0.14

surfaces exposed to 27 kJ of air plasma had the highest affinity to GFP, that enabled the immobilization of GFP with high surface density within the fixed time constraint of the EDC–NHS reaction. While the PMMA surfaces treated with 27 kJ air plasma were saturated with GFP when $C_0 > 0.93$ μM, it was observed that the maximum fractional coverage achieved (f_B) was only 72% of the total available sites (Q_{max}).

The distribution of GFP on the PMMA surfaces can be predicted by analyzing the value of n, that determines if the binding of GFP to PMMA is positively cooperative ($n > 1$), negatively cooperative ($n < 1$), or independent of other binding events ($n = 1$). The average value of n for the PMMA surfaces were less than 1 ($n = 0.44 \pm 0.03$), independent of plasma energy (Table 4). This indicates that the binding of one GFP molecule to the PMMA surface decreases the binding affinity of the next GFP molecule. Although the surfaces of GFP are relatively hydrophobic, the negative cooperativity between plasma-treated PMMA activated with EDC–NHS and GFP binding prevented close packing and formation of multilayer aggregates of GFP at the chosen initial GFP concentrations. Additionally, steric hindrance could potentially add to the inability to completely saturate all available binding sites (Q_{max}). Nevertheless, significantly high GFP surface densities were obtained when coupled with PMMA surfaces exposed to 27 kJ air plasma and treated with EDC–NHS with relatively low initial concentrations of GFP. Furthermore, the proposed PMMA biofunctionalization method proved to be efficient in immobilizing multiple kinds of biomolecules, namely, IgGs and streptavidin, two commonly employed biomolecules for functionalization of biosensors. The fractions of specifically chemisorbed IgG and streptavidin on treated PMMA were found to be 0.8 and 0.9 respectively, thereby validating the specificity of our proposed PMMA biofunctionalization strategy (Figure S6). In section 3.4, we demonstrate the applicability of this strategy to functionalize microfluidic bioassay devices with major outer membrane proteins (MOMP) for the detection of antibodies specific to *Chlamydia trachomatis*.

3.3. Preserved GFP Biofunctionality When Chemisorbed on PMMA. The extent of the preservation of protein structures upon immobilization determines their analyte binding efficiencies and sensitivities. The structure of the immobilized GFP is dependent on not only the type of surface interactions (hydrophobic vs covalent) but also the protein environment.[8] Specifically, the pH of the protein solution heavily influences both the structural and functional integrity of protein structures and the specificity of covalent interactions. Several studies have demonstrated that the fluorescence emission efficiency of GFP, determined by its structure, is highly sensitive to the pH of the solution. Therefore, the change in GFP fluorescence emission when chemisorbed on EDC–NHS-activated PMMA exposed to 27 kJ air plasma as a function of pH was investigated and correlated with the biofunctionality of the immobilized GFP.

For this study, GFP was immobilized on activated PMMA using two different solutions with different buffering capacities: (i) neutral PBS buffer (pH 7.4), and (ii) acidic MES buffer (pH 6). To achieve the most efficient EDC–NHS mediated covalent coupling of proteins and substrates, the conventional rule of thumb is to perform the coupling reactions at a pH less than the isoelectric point (pI) of the protein. In these conditions, the protein surfaces are positively charged and are able to react with the negatively charged carboxyl groups. Here, a pH of 6 was chosen to achieve maximum covalent coupling efficiency, as the pI of GFP is around 5.8. A pH of 6 was chosen since, at lower pH, GFP molecular restructuring has been observed that leads to changes in its biophysical properties.[39] As seen in Figure 3a, with the same initial GFP concentrations (C_0), the normalized fluorescence intensity (section 2.4) of chemisorbed GFP on activated PMMA (27 kJ air plasma) at pH 6 is significantly lower than when chemisorbed at a pH of 7.4. Additionally, the fluorescence intensity of chemisorbed GFP was seen to reach saturation at $C_0 > 1.2$ μM for both conditions. However, the saturation fluorescence intensity was 2-fold lower for GFP chemisorbed at pH 6 when compared to pH 7.4. To investigate if the decreases in fluorescence intensity was a result of lower efficiency of covalent coupling, surface adsorption studies were performed. The GFP surface densities (q) were extracted from the fluorescence intensities for the respective conditions, to investigate the differences in surface saturation using the Hill–Langmuir equation (eq 8). The fraction of total active sites ($Q_{max} = 5.8 \times 10^{-6}$, Figure 2a) bound by GFP ($f_B = q/Q_{max}$) after a reaction time of 15 min, was 3-fold higher (Figure 3b), while K_A was reduced for GFP chemisorbed at pH 7.4 (Table 5), demonstrating that the affinity of the activated PMMA

Table 5. Hill–Langmuir Equation Parameters for GFP Chemisorption on EDC–NHS-Activated PMMA Exposed to 27 kJ Air Plasma as a Function of pH

pH	K_A (μM)	n
7.4 (PBS buffer)	0.23 ± 0.07	0.54 ± 0.14
6 (MES buffer)	5.62 ± 2.14	0.85 ± 0.20

surfaces for GFP chemisorption was higher at pH 7.4. While the differences in chemisorption efficiency at pH 6 and 7.4 are indicative of the differences in efficiencies of covalent interactions, the surface adsorption study could not directly determine if structural changes of GFP occurred during the chemisorption process.

As any structural changes of GFP would impede its ability to bind to specific binding partners, binding studies were performed to investigate the biofunctionality of chemisorbed GFP as a function of pH. Varying initial concentrations of GFP were chemisorbed on EDC–NHS-activated PMMA exposed to 27 kJ air plasma at pH 6 and 7.4, for 15 min. Following blocking of unbound sites on PMMA, fixed concentrations of fluorescent anti-GFP immunoglobulin G (IgG) were added to bind to the chemisorbed GFP (Figure 3c). As seen in Figure 3d, the fluorescence intensity of bound IgG–GFP complex increases logistically as a function of GFP surface-density for GFP chemisorbed at pH 7.4. In contrast, the IgG–GFP complex formation was seen to be independent of GFP surface density, for GFP chemisorbed at pH 6 (inset of Figure 3d). These results indicate that GFP chemisorbed at pH 7.4 retains its structural integrity while maintaining its binding capacity.

DOI: 10.1021/acsami.9b14631
ACS Appl. Mater. Interfaces 2019, 11, 46350–46360

However, the efficiency of IgG to bind to GFP chemisorbed at pH 6 was lower than pH 7.4, indicating that chemisorption at pH 6 leads to structural changes of GFP, as predicted by previous studies.[40,41]

Hence, the decrease in fluorescence intensity appeared to be a result of the combined effect of structural alterations at pH 6 that lead to lower covalent coupling efficiencies when chemisorbed on activated PMMA. Although the pH of the reaction can be manipulated to increase the coupling efficiency, the structural integrity of the protein is lost as a consequence. Additionally, we observed that GFP was immobilized onto treated PMMA surfaces with a layer thickness of ∼20 nm, at pH 6 (Figure S7). This indicates the presence of approximately 5 layers of GFP molecules, given that the average height of one GFP molecule is ∼4.2 nm.[42] In parallel, an ∼18 nm thick layer of IgG indicated the binding of 2 layers of IgGs with sideways orientation (average thickness of 1 IgG molecule = 8.5 nm).[43] Therefore, we demonstrated that high surface densities of structurally preserved, chemisorbed proteins can be achieved on activated PMMA surfaces, by choosing a more neutral protein environment, vis-à-vis, the protein buffer.

3.4. Microfluidic PMMA Device to Detect Chlamydia-Specific IgGs. The development of coupled microarray and microfluidic technology has boosted the creation of miniaturized and disposable high-throughput screening chips that enable parallel analyses of biochemical compounds with limited reagent quantities and short detection times.[44−46] The robust mechanical and optical properties of PMMA has made this thermoplastic a popular candidate for the fabrication of these chips.[47] However, the lack of scalable and reproducible chemical modification techniques that enable controlled immobilization of proteins with preserved functionalities has hindered the development of PMMA-based microfluidic-microarray chips.

By exploiting our tailored air plasma-enhanced PMMA covalent functionalization process, we demonstrated a proof-of-concept microfluidic bioassay to detect clinically significant concentrations of immunoglobulins (IgGs) specific to *Chlamydia trachomatis* infections. Clinical research has shown that bacterial *C. trachomatis* infections are the most prevalent sexually transmitted infections, contributing to high rates of miscarriages and infertility worldwide. During several immunization studies,[48,49] it was observed that the antigenic major outer membrane protein (MOMP) of *C. trachomatis*, induced the highest immune response, with anti-MOMP IgG secretions (25 pM−25 μM) detected in the blood serum. Therefore, we chemisorbed MOMP fragments (C_0 = 1.25 μM) on EDC−NHS-treated PMMA substrates exposed to 27 kJ air plasma at pH 7.4 that served as the capture biomolecules in the subsequent IgG assay (inset of Figure 4a).

The MOMP-chemisorbed PMMA substrates were bonded to bare PMMA substrates, using double-sided (ds) adhesive tapes consiting of carbon dioxide laser etched microchannels (Figure 4a). The ds tape served as the channel walls, with the thickness (53 μm) contributing to the overall microchannel height. The bare surfaces of the PMMA microchannels were blocked with BSA to prevent non-specific adsorption. Either human plasma samples diluted with PBS (1:2) or PBS buffer samples (100 μL) doped with varying concentrations of anti-MOMP IgGs (0.83−13.3 nM) were manually pipetted into the inlet of the microchannels to mimic an "off-the-shelf" bioassay chip. The IgGs captured by MOMP were visualized via fluorescence microscopy, with the help of complementary fluorescently labeled IgGs, pipetted into the channels. Figure 4b,c, depict that the MOMP-functionalized PMMA microfluidic devices enabled the successful capture and detection of linearly increasing concentrations anti-MOMP IgGs. The inhomogeneity of the fluorescence intensity in Figure 4c is due to the cumulative influence of the nonuniform PMMA substrate and ds tape autofluorescence, observed in the tetramethylrhodamine (TRITC) excitation and emission wavelengths during fluorescence imaging. The favorable capture and detection of anti-MOMP IgGs by the MOMP-functionalized PMMA microfluidic devices, confirms that the structural integrity of MOMP is maintained when immobilized on EDC−NHS-treated PMMA microfluidic channels, activated by air plasma. Although the anti-MOMP IgGs could be detected within 15 min from PBS samples, an incubation time of 1 h was required to reliably detect the same range of concentrations from the diluted human plasma samples, owing to the increased proportion of competing proteins in human plasma.

The efficiency of the microfluidic system was characterized by calculating the limit of detection (LoD) and limit of quantification (LoQ) of the systems, using the following equations:[50]

$$\mathrm{LoD} = 3.3(\mathrm{SD}_{(\mathrm{int})}/s) \tag{9}$$

$$\mathrm{LoQ} = 10(\mathrm{SD}_{(\mathrm{int})}/s) \tag{10}$$

where, $\mathrm{SD}_{(\mathrm{int})}$ and s are the standard deviations of the y-intercept and the slopes of the linear fit, respectively (black solid line in Figure 4b). The lowest concentration of anti-MOMP IgGs that could be detected in the PBS samples using the microfluidic device (i.e., LoD) was estimated to be 1.35 nM, and the lowest concentration that could be reliably quantified (i.e., LoQ) was 4.09 nM, 3-fold higher than the LoD. However, the LoD and LoQ of the microfluidic systems were higher for the human plasma samples, owing to the complex nature of the samples (LoD = 2.67 nM, LoQ = 8.08 nM). Nevertheless, the LoQ of the MOMP-chemisorbed, manually controlled microfluidic chips was within the clinically significant anti-MOMP IgG concentration range (25 pM−25 μM),[48,49] irrespective of the type of fluid sample. The proof-of-concept microfluidic bioassay device demonstrates the potential of exploiting our simple yet scalable surface functionalization process, to create reproducible PMMA microfluidic protein screening chips, on a large-scale. Additionally, the LoD and LoQ can be significantly improved not only by optimizing the microfluidic device geometric and flow parameters but also by exploiting more sensitive detection mechanisms in the future.

4. CONCLUSIONS

Immobilization of proteins onto plastic surfaces such as PMMA is primarily driven by hydrophobic interactions. This entails that hydrophobic proteins have higher affinity to PMMA than hydrophilic proteins. However, hydrophobic interaction-driven immobilization not only causes high non-specific adsorption of proteins but also leads to protein unfolding to expose hydrophobic residues. In contrast, covalent interactions exploit the surface properties of both, the protein and PMMA surfaces. However, the surfaces of PMMA are inert and require stringent surface manipulations to render the surfaces functional for immobilization of proteins. Here, we demonstrated a simple and rapid method exploiting

DOI: 10.1021/acsami.9b14631
ACS Appl. Mater. Interfaces 2019, 11, 46350−46360

the ability of air plasma to generate activated carboxyl groups on PMMA that enabled covalent coupling of GFP via EDC−NHS mediated chemistry while reducing non-specific adsorption. We observed that the GFP immobilization efficiency was dependent on the plasma energy, where the surfaces exposed to 27 kJ of air plasma were seen to have a good mixture of polar and hydrophobic groups, which resulted in maximum affinity for GFP immobilization, requiring lower concentrations of GFP to achieve surface saturation.

Owing to the time-sensitive EDC−NHS reaction, the ability to achieve high GFP surface density with lower initial concentrations of GFP, is immensely advantageous, as it could enable the fabrication of reagent-friendly bioassay substrates with ease. Additionally, we demonstrated that the immobilization efficiency and biofunctionality of the immobilized GFP is pH-dependent. GFP immobilized at a more neutral pH (pH 7.4) was shown not only to enable high GFP surface density but also to allow efficient binding with anti-GFP IgG, thereby demonstrating the preservation of GFP biofunctionality after immobilization on to PMMA. We demonstrated the applicability of the proposed strategy for specific chemisorption of a wide range of biomolecules, namely, IgGs, streptavidin and major outer membrane proteins (MOMP) of *C. trachomatis*. Finally, the optimized functionalization method was exploited to fabricate microfluidic antibody assay devices to detect clinically significant concentrations of antibodies specific to *C. trachomatis*. By reliably immobilizing both GFP and MOMP fragments on EDC−NHS-activated air plasma-treated PMMA substrates, we present the potential applicability of the demonstrated strategy for covalent functionalization of PMMA with different families of proteins.

Conventional methods for functionalizing plastic surfaces with proteins to create disease diagnostic tools such as ELISA plates and microfluidic chips rely on methods that are difficult to scale up for industrial applications. Our rapid and scalable, yet controlled, biofunctionalization method serves as a benchmark platform to fabricate reproducible, high-throughput protein screening systems, further driving innovations in chemical and biochemical screening assays.

■ ASSOCIATED CONTENT

Supporting Information

The Supporting Information is available free of charge at https://pubs.acs.org/doi/10.1021/acsami.9b14631.

GFP surface density standard curve (Figure S1); surface roughness of PMMA (Figure S2); Owens, Wendt, Rabel, and Kaelble (OWRK) model for calculation of surface energy of PMMA (Figure S3); X-ray photoelectron spectroscopy (XPS) analysis of PMMA surface (Figure S4); relationship between surface density and initial concentrations of GFP (Figure S5); specific immobilization of multiple biomolecules on treated PMMA (Figure S6); thickness of biomolecular layers on treated PMMA (Figure S7) (PDF)

■ AUTHOR INFORMATION

Corresponding Author

*E-mail: amy.shen@oist.jp.

ORCID

Shivani Sathish: 0000-0001-8082-1914

Amy Q. Shen: 0000-0002-1222-6264

Notes

The authors declare no competing financial interest.

■ ACKNOWLEDGMENTS

S.S. is a JSPS DC2 fellow (Japan Society of Promotion for Science) and this work is supported by JSPS KAKENHI [Grant Number 19J11009]. A.Q.S also acknowledges financial support from JSPS under grants 17K06173 and 18H01135. We thank Okinawa Institute of Science and Technology Graduate University (OIST) and the OIST "Proof-of-Concept initiative" for their financial support, with subsidy funding from the Cabinet Office, Government of Japan. We thank Dr. David Vazquez Cortes and Mr. Kazumi Toda-Peters for technical assistance. We also thank Dr. Vikash Chaurasia and Dr. Stoffel Janssens for useful scientific discussions.

■ REFERENCES

(1) Chen, Z.; Dodig-Crnković, T.; Schwenk, J. M.; Tao, S.-c. Current applications of antibody microarrays. *Clin. Proteomics* **2018**, *15*, 7.

(2) Luka, G.; Ahmadi, A.; Najjaran, H.; Alocilja, E.; DeRosa, M.; Wolthers, K.; Malki, A.; Aziz, H.; Althani, A.; Hoorfar, M. Microfluidics integrated biosensors: A leading technology towards lab-on-a-chip and sensing applications. *Sensors* **2015**, *15*, 30011−30031.

(3) Zhong, Q.; Ding, H.; Gao, B.; He, Z.; Gu, Z. Advances of Microfluidics in Biomedical Engineering. *Advanced Materials Technologies* **2019**, *4*, 1800663.

(4) Lim, H. G.; Jang, S.; Jang, S.; Seo, S. W.; Jung, G. Y. Design and optimization of genetically encoded biosensors for high-throughput screening of chemicals. *Curr. Opin. Biotechnol.* **2018**, *54*, 18−25.

(5) Du, G.; Fang, Q.; den Toonder, J. M. Microfluidics for cell-based high throughput screening platforms − A review. *Anal. Chim. Acta* **2016**, *903*, 36−50.

(6) Carvalho, R. R.; Pujari, S. P.; Vrouwe, E. X.; Zuilhof, H. Mild and Selective C−H Activation of COC Microfluidic Channels Allowing Covalent Multifunctional Coatings. *ACS Appl. Mater. Interfaces* **2017**, *9*, 16644−16650.

(7) Wan, A. M.; Devadas, D.; Young, E. W. Recycled polymethylmethacrylate (PMMA) microfluidic devices. *Sens. Actuators, B* **2017**, *253*, 738−744.

(8) Wild, D. *The Immunoassay Handbook: Theory and Applications of Ligand Binding, ELISA and Related Techniques*; Newnes, 2013.

(9) Fixe, F.; Dufva, M.; Telleman, P.; Christensen, C. B. V. Functionalization of poly (methyl methacrylate)(PMMA) as a substrate for DNA microarrays. *Nucleic Acids Res.* **2004**, *32*, No. 9e.

(10) Yang, P.; Zhang, X.; Yang, B.; Zhao, H.; Chen, J.; Yang, W. Facile Preparation of a Patterned, Aminated Polymer Surface by UV-Light-Induced Surface Aminolysis. *Adv. Funct. Mater.* **2005**, *15*, 1415−1425.

(11) Punet, X.; Mauchauffe, R.; Rodríguez-Cabello, J. C.; Alonso, M.; Engel, E.; Mateos-Timoneda, M. A. Biomolecular functionalization for enhanced cell−material interactions of poly (methyl methacrylate) surfaces. *Regenerative Biomaterials* **2015**, *2*, 167−175.

(12) Hosseini, S.; Ibrahim, F.; Djordjevic, I.; Koole, L. H. Recent advances in surface functionalization techniques on polymethacrylate materials for optical biosensor applications. *Analyst* **2014**, *139*, 2933−2943.

(13) Ortiz, R.; Chen, J. L.; Stuckey, D. C.; Steele, T. W. Poly (methyl methacrylate) surface modification for surfactant-free real-time toxicity assay on droplet microfluidic platform. *ACS Appl. Mater. Interfaces* **2017**, *9*, 13801−13811.

(14) Vesel, A.; Mozetic, M. New developments in surface functionalization of polymers using controlled plasma treatments. *J. Phys. D: Appl. Phys.* **2017**, *50*, 293001.

(15) Shakeri, A.; Imani, S. M.; Chen, E.; Yousefi, H.; Shabbir, R.; Didar, T. F. Plasma-induced covalent immobilization and patterning

DOI: 10.1021/acsami.9b14631
ACS Appl. Mater. Interfaces 2019, 11, 46350−46360

of bioactive species in microfluidic devices. *Lab Chip* **2019**, *19*, 3104−3115.
(16) Diaz-Quijada, G. A.; Peytavi, R.; Nantel, A.; Roy, E.; Bergeron, M. G.; Dumoulin, M. M.; Veres, T. Surface modification of thermoplastics − towards the plastic biochip for high throughput screening devices. *Lab Chip* **2007**, *7*, 856−862.
(17) Vesel, A.; Elersic, K.; Mozetic, M. Immobilization of protein streptavidin to the surface of PMMA polymer. *Vacuum* **2012**, *86*, 773−775.
(18) Long, T. M.; Prakash, S.; Shannon, M. A.; Moore, J. S. Water-vapor plasma-based surface activation for trichlorosilane modification of PMMA. *Langmuir* **2006**, *22*, 4104−4109.
(19) Kang, I.-K.; Kwon, B. K.; Lee, J. H.; Lee, H. B. Immobilization of proteins on poly (methyl methacrylate) films. *Biomaterials* **1993**, *14*, 787−792.
(20) Liu, C.; Wu, J.; Ren, L.; Tong, J.; Li, J.; Cui, N.; Brown, N.; Meenan, B. Comparative study on the effect of RF and DBD plasma treatment on PTFE surface modification. *Mater. Chem. Phys.* **2004**, *85*, 340−346.
(21) Rezaei, F.; Shokri, B.; Sharifian, M. Atmospheric-pressure DBD plasma-assisted surface modification of polymethyl methacrylate: A study on cell growth/proliferation and antibacterial properties. *Appl. Surf. Sci.* **2016**, *360*, 641−651.
(22) Klébert, S.; Károly, Z.; Késmárki, A.; Domján, A.; Mohai, M.; Keresztes, Z.; Kutasi, K. Solvent-and catalysts-free immobilization of tannic acid and polyvinylpyrrolidone onto PMMA surface by DBD plasma. *Plasma Processes Polym.* **2017**, *14*, 1600202.
(23) Johansson, B.-L.; Larsson, A.; Ocklind, A.; Öhrlund, Å. Characterization of air plasma-treated polymer surfaces by ESCA and contact angle measurements for optimization of surface stability and cell growth. *J. Appl. Polym. Sci.* **2002**, *86*, 2618−2625.
(24) De Michele, C.; De Los Rios, P.; Foffi, G.; Piazza, F. Simulation and theory of antibody binding to crowded antigen-covered surfaces. *PLoS Comput. Biol.* **2016**, *12*, No. e1004752.
(25) Tsai, H.-F.; Cheng, J.-Y.; Chang, H.-F.; Yamamoto, T.; Shen, A. Q. Uniform electric field generation in circular multi-well culture plates using polymeric inserts. *Sci. Rep.* **2016**, *6*, 26222.
(26) Prasher, D. C.; Eckenrode, V. K.; Ward, W. W.; Prendergast, F. G.; Cormier, M. J. Primary structure of the Aequorea victoria green-fluorescent protein. *Gene* **1992**, *111*, 229−233.
(27) Crone, D. E.; Huang, Y.-M.; Pitman, D. J.; Schenkelberg, C.; Fraser, K.; Macari, S.; Bystroff, C. *State of the Art in Biosensors-General Aspects*; IntechOpen, 2013.
(28) Chai, J.; Lu, F.; Li, B.; Kwok, D. Y. Wettability interpretation of oxygen plasma modified poly (methyl methacrylate). *Langmuir* **2004**, *20*, 10919−10927.
(29) Kwok, D. Y.; Neumann, A. W. Contact angle measurement and contact angle interpretation. *Adv. Colloid Interface Sci.* **1999**, *81*, 167−249.
(30) Annamalai, M.; Gopinadhan, K.; Han, S. A.; Saha, S.; Park, H. J.; Cho, E. B.; Kumar, B.; Patra, A.; Kim, S.-W.; Venkatesan, T. Surface energy and wettability of van der Waals structures. *Nanoscale* **2016**, *8*, 5764−5770.
(31) Senturk Parreidt, T.; Schmid, M.; Hauser, C. Validation of a novel technique and evaluation of the surface free energy of food. *Foods* **2017**, *6*, 31.
(32) Xia, H.; Murray, K.; Soper, S.; Feng, J. Ultra sensitive affinity chromatography on avidin-functionalized PMMA microchip for low abundant post-translational modified protein enrichment. *Biomed. Microdevices* **2012**, *14*, 67−81.
(33) Cowie, J. M.; Mohsin, M. A.; McEwen, I. J. Alcohol-water cosolvent systems for poly (methyl methacrylate). *Polymer* **1987**, *28*, 1569−1572.
(34) Kawai, J.; Adachi, H.; Kitajima, Y.; MAEDA, K.; HAYAKAWA, S.; GoHSHI, Y. Inelastic mean free path of photoelectrons in Ag determined by total reflection X-ray photoelectron spectroscopy. *Anal. Sci.* **1997**, *13*, 797−801.
(35) He, X.; Male, K. B.; Nesterenko, P. N.; Brabazon, D.; Paull, B.; Luong, J. H. Adsorption and desorption of methylene blue on porous carbon monoliths and nanocrystalline cellulose. *ACS Appl. Mater. Interfaces* **2013**, *5*, 8796−8804.
(36) Welsch, N.; Lu, Y.; Dzubiella, J.; Ballauff, M. Adsorption of proteins to functional polymeric nanoparticles. *Polymer* **2013**, *54*, 2835−2849.
(37) Genzer, J. *Soft Matter Gradient Surfaces: Methods and Applications*; John Wiley & Sons, 2012.
(38) Hill, E. H.; Zhang, Y.; Evans, D. G.; Whitten, D. G. Enzyme-specific sensors via aggregation of charged p-phenylene ethynylenes. *ACS Appl. Mater. Interfaces* **2015**, *7*, 5550−5560.
(39) Elsliger, M.-A.; Wachter, R. M.; Hanson, G. T.; Kallio, K.; Remington, S. J. Structural and spectral response of green fluorescent protein variants to changes in pH. *Biochemistry* **1999**, *38*, 5296−5301.
(40) Campbell, T. N.; Choy, F. Y. The effect of pH on green fluorescent protein: a brief review. *Mol. Biol. Today* **2001**, *2*, 1−4.
(41) Nii, D.; Nozawa, Y.; Miyachi, M.; Yamanoi, Y.; Nishihara, H.; Tomo, T.; Shimada, Y. Peptide aptamer-assisted immobilization of green fluorescent protein for creating biomolecule-complexed carbon nanotube device. *Jpn. J. Appl. Phys.* **2017**, *56*, 107001.
(42) Hink, M. A.; Griep, R. A.; Borst, J. W.; Van Hoek, A.; Eppink, M. H.; Schots, A.; Visser, A. J. Structural dynamics of green fluorescent protein alone and fused with a single chain Fv protein. *J. Biol. Chem.* **2000**, *275*, 17556−17560.
(43) Tan, Y. H.; Liu, M.; Nolting, B.; Go, J. G.; Gervay-Hague, J.; Liu, G.-y. A nanoengineering approach for investigation and regulation of protein immobilization. *ACS Nano* **2008**, *2*, 2374−2384.
(44) Sathish, S.; Ricoult, S. G.; Toda-Peters, K.; Shen, A. Q. Microcontact printing with aminosilanes: creating biomolecule micro- and nanoarrays for multiplexed microfluidic bioassays. *Analyst* **2017**, *142*, 1772−1781.
(45) Valles, D. J.; Naeem, Y.; Carbonell, C.; Wong, A. M.; Mootoo, D. R.; Braunschweig, A. B. Maskless Photochemical Printing of Multiplexed Glycan Microarrays for High-Throughput Binding Studies. *ACS Biomater. Sci. Eng.* **2019**, *5*, 3131−3138.
(46) Alqurashi, T.; Alnufaili, M.; Hassan, M. U.; Aloufi, S.; Yetisen, A. K.; Butt, H. Laser Inscription of Microfluidic Devices for Biological Assays. *ACS Appl. Mater. Interfaces* **2019**, *11*, 12253−12260.
(47) Al-aqbi, Z. T.; Yap, Y. C.; Li, F.; Breadmore, M. C. Integrated Microfluidic Devices Fabricated in Poly (Methyl Methacrylate)-(PMMA) for On-site Therapeutic Drug Monitoring of Aminoglycosides in Whole Blood. *Biosensors* **2019**, *9*, 19.
(48) Badamchi-Zadeh, A.; McKay, P. F.; Holland, M. J.; Paes, W.; Brzozowski, A.; Lacey, C.; Follmann, F.; Tregoning, J. S.; Shattock, R. J. Intramuscular immunisation with chlamydial proteins induces Chlamydia trachomatis specific ocular antibodies. *PLoS One* **2015**, *10*, No. e0141209.
(49) Badamchi-Zadeh, A.; McKay, P. F.; Korber, B. T.; Barinaga, G.; Walters, A. A.; Nunes, A.; Gomes, J. P.; Follmann, F.; Tregoning, J. S.; Shattock, R. J. A multi-component prime-boost vaccination regimen with a consensus MOMP antigen enhances Chlamydia trachomatis clearance. *Front. Immunol.* **2016**, *7*, 162.
(50) Shrivastava, A.; Gupta, V. B. Methods for the determination of limit of detection and limit of quantitation of the analytical methods. *Chronicles of Young Scientists* **2011**, *2*, 21−25.

DOI: 10.1021/acsami.9b14631
ACS Appl. Mater. Interfaces 2019, 11, 46350−46360